Journal of Physical Science, Vol. 34(2), 75–89, 2023

Annealing Temperature Dependence on Magnetic Properties, Crystalline Structure and Photocatalyst Activity of Coprecipitated Cobalt Ferrite ($CoFe_2O_4$) Synthesised from Natural Iron Sand

Budi Purnama,[1*] Arga Dwi Suwandi,[1] Rudi Hartono,[2] Sahirul Alim Tri Bawono,[2] Utari Utari,[1] Herman Aldila,[3] Adi Rahwanto[4] and Kusumandari Kusumandari[1*]

[1]Department of Physics, Faculty of Mathematics and Natural Sciences, Universitas Sebelas Maret, Jalan Ir. Sutami 36A Kentingan Surakarta 57126, Indonesia
[2]Department of Informatics Engineering, Universitas Sebelas Maret, Jl. Ir. Sutami 36A Kentingan Jebres Surakarta 57126, Indonesia
[3]Department of Physics, Universitas Bangka Belitung, Gang IV No.1, Balun Ijuk, Merawang, Kabupaten Bangka, Kepulauan Bangka Belitung 33172, Indonesia
[4]Department of Physics, Syiah Kuala University, Jl. Teuku Nyak Arief No.441, Kopelma Darussalam, Kec. Syiah Kuala, Kota Banda Aceh, Aceh 23111, Indonesia

[*]Corresponding authors: bpurnama@mipa.uns.ac.id, kusumandari@staff.uns.ac.id

Published online: 25 August 2023

To cite this article: Purnama, B. et al. (2023). Annealing temperature dependence on magnetic properties, crystalline structure and photocatalyst activity of coprecipitated cobalt ferrite ($CoFe_2O_4$) using natural iron sand. *J. Phys. Sci.*, 34(2), 75–89. https://doi.org/10.21315/jps2023.34.2.6

To link to this article: https://doi.org/10.21315/jps2023.34.2.6

ABSTRACT: *Cobalt ferrite ($CoFe_2O_4$) nanopowder was successfully synthesised by the coprecipitation method. For the entire experiment, natural iron sand from the Bengawan Solo River is used as an iron (Fe) cation source. The effect of the annealing temperature of a coprecipitated $CoFe_2O_4$ sample from natural iron sand was investigated. The presence of strong metal oxide bond groups at the tetrahedral and octahedral sites is revealed by fourier transform infrared (FTIR) spectral results, owing to the $CoFe_2O_4$ characteristic. Then the X-ray diffraction (XRD) pattern confirmed the formation of a single-phase $CoFe_2O_4$ with face centred cubic (FCC) crystal structure closely matched to reference data ICDD221086. The crystalline parameters such as lattice parameter and crystallite size modify with the increase of annealing temperature. The saturation magnetisation (Ms) decreases as the annealing temperature rises. In addition, the coercive fields (Hc) increases as the annealing temperature rises. As a result, the annealing temperature affects the performance of the $CoFe_2O_4$ photocatalyst. The photocatalytic performance of the annealing temperature sample at 300°C was found to be the best.*

Keywords: iron sand, cobalt ferrite, coprecipitation, annealing, photocatalyst

1. INTRODUCTION

Recently, researchers and scientists are interested in spinel ferrite magnetic materials in the form of nanopowder scale as well as thin-film because of their appearance-interesting properties.[1–6] Cobalt ferrite ($CoFe_2O_4$) is one of the spinel ferrite magnetic materials which has a face-centered cubic (FCC) crystal structure Fd-3 m space group. In general, inverse spinel $CoFe_2O_4$ has a formula $Co^{2+}(Fe^{3+})_2O_4$, with Co^{2+} being a divalent cation occupying an octahedral site while iron(iii) (Fe^{3+}) is a trivalent cation that occupies both tetrahedral and octahedral site.[7–9] However, the observed inversion degree (δ) is often less than 1 for Co^{2+}.Co^{2+} ions occupy the octahedral sites in bulk $CoFe_2O_4$ while Co^{2+} occupies both the tetrahedral and octahedral sites in nano-size order materials.[10–12] $CoFe_2O_4$ has interesting properties i.e., high magnetocrystalline anisotropy (~3×10^5 J/m^3), large coercivity at room temperature (~5.4 kOe) and moderate saturation magnetisation (Ms) (~87 emu/g).[13,14] As a result, it has a high potential for use in a variety of technologies, including magnetic hyperthermia, antibacterial, drug delivery and photocatalyst.[4–6,15]

Today, research based on natural materials has attracted a lot of attention because it's environmentally friendly. Regarding $CoFe_2O_4$, several studies show that it can be synthesised using natural plant extracts as previously reported.[16,17] Also, there are some early studies that natural iron sand can replace Fe^{3+} ions in the synthesis of lead hexaferrite powder, magnesium ferrite powder and $CoFe_2O_4$ powder.[18–20] Moreover, some researchers have modified the properties of $CoFe_2O_4$ of a such kind by adding dopant bismuth (Bi), variations in annealing temperature and synthesis methods to get suitable properties of $CoFe_2O_4$. Based on the abundance of natural iron sand in Indonesia, which has not been fully explored, there are interesting challenges in researching the preparation of $CoFe_2O_4$ and its modification.[9,21,22]

Chemical synthesis methods widely used for the preparation of $CoFe_2O_4$ include sol-gel, hydrothermal, auto-combustion and coprecipitation methods.[23–26] This method is widely used because it can be carried out at room temperature and is simple.[27,28] Among these methods, the coprecipitation method is advantageous for synthesising nanoparticles due to the use of inexpensive materials, low energy requirements, uniformity in particle size, simple experimental conditions and easily soluble impurities removed.[28,29]

In this study, $CoFe_2O_4$ was synthesised by the coprecipitation method using natural iron sand as a Fe cation source with the variation of annealing temperature. The $CoFe_2O_4$ was characterised using fourier transform infrared (FTIR), X-ray diffractometer (XRD) and vibrating sample magnetometer (VSM) to determine the chemical bonding group, crystal structure and magnetic properties, respectively.

Meanwhile, the photocatalytic activity of the $CoFe_2O_4$ samples were evaluated using UV-Vis characterisation.

2. EXPERIMENTAL

The natural iron sand was taken from the Bengawan Solo River, Bojonegoro, East Java, Indonesia. Whereas the preparation of natural iron sand as a Fe cation source follows the procedure as reported previously.[30] First, the amount stoichiometry of $Co(NO_3)_2.6H_2O$ (Merck) and iron sand was dissolved in 200 ml of distilled water. The mixed solution was then heated to 95°C while being stirred at 300 rpm for 20 min. Following that, a 4.8 M NaOH solution was added dropwise to the mixed solution until a black precipitate formed. The precipitate product was then washed with ethanol and distilled water. The precipitate product then was dried in the oven at 100°C for 12 h. Next, the obtained products were crushed for 1 h, then annealed at different temperatures (300°C, 400°C and 500°C) for 4 h. To investigate the chemical bonding group, the final product of samples was characterised using an FTIR spectrophotometer. XRD with Cu-$K\alpha_1$ (1.5406 Å) radiation was used to evaluate the phase material and crystal structure. The lattice parameter *a* for the cubic structure was evaluated using the Bragg Equation as shown below:[31]

$$d = \frac{a}{\sqrt{h^2 + k^2 + l^2}} = \frac{\lambda}{2 \sin \theta} \tag{1}$$

The lattice strain $\sum$ was calculated following the equation:[32]

$$\Sigma = \frac{\beta \, hkl}{4 \tan \theta} \tag{2}$$

The crystallite size *D* of all samples determines using the strongest peak of the XRD graph with the Debye Scherrer equation.[32]

$$D = \frac{k\lambda}{\beta \cos \theta} \tag{3}$$

With λ is the wavelength of the Cu-Kα source and refers to the full width at half the maximum of the concerned peak. The crystalline density d_x is calculated following the equation:[33]

$$d_x = \frac{8M}{Na^3} \tag{4}$$

Where M is the molecular weight, N is Avogadro's number, is the lattice parameter and d_x is the density. The magnetic properties were investigated using a VSM. Calculation of the total magnetic moment using the formula.[34]

$$n_B = \frac{M_A \times M_S}{N_A \times 9.27 \times 10^{-21}} \tag{5}$$

With M_A and N_A are molecular weight and Avogadro's number. Finally, the photocatalytic activity of $CoFe_2O_4$ was evaluated using the degradation of methylene blue (MB) (after 10 min of UV irradiation) based on its absorbance measured using a UV-Visible spectrophotometer. It is well known that absorbance is related to the number of pollutants. Therefore, the degradation efficiency was evaluated using a comparison of the maximum absorbance of MB with and without adding powder $CoFe_2O_4$. It was calculated using Equation (6) as follows:[35]

$$\text{Degradation efficiency} = \frac{A_0 - A_t}{A_0} \times 100\% \tag{6}$$

In this study, the kinetic rate constant was calculated using the first-order kinetics reaction model equation defined as:

$$\ln\left(\frac{A_t}{A_o}\right) = kt \tag{7}$$

With t is irradiation time, A_0 is the initial absorbance and A_t is the absorbance of MB after adding powder $CoFe_2O_4$ at time t, respctively.[21]

3. RESULTS AND DISCUSSION

Figure 1 shows the XRD diffraction pattern of coprecipitated $CoFe_2O_4$ at different annealing temperatures of 300°C, 400°C and 500°C. It can be seen that the peaks of all samples were well indexed with reference standard ICDD number 221086 namely (220), (311), (222), (400), (422), (511) and (440) which according to a face-centered cubic crystal structure with the Fd-3 m space group. The absence of impurity peaks confirms that the synthesis of coprecipitated $CoFe_2O_4$ with natural iron sand is a single-phase and still retains the spinel crystal structure. Furthermore, the strongest peak (311) shifted to a higher angle as the annealing temperature increased. It indicates a decrease in lattice parameter a which will be discussed later. This finding is consistent with the previous study.[26] Table 1 shows

the resume of a crystalline parameter such as lattice parameter (a), strain lattice ($\sum$), the crystallite size (D) and crystalline density (d_x). The a can be explained using Equation (1). The $\sum$ was calculated following Equation (2). While the D was determined using the strongest peak (311) via Equation (3). The d_x is calculated using Equation (4).

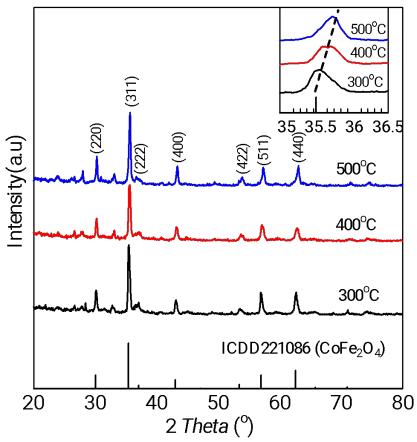

Figure 1: XRD pattern of $CoFe_2O_4$ nanopowder for different annealing temperatures of 300°C, 400°C and 500°C.

Table 1: Lattice parameter (a), crystallite size (D), crystalline density (dx) and lattice strain (Σ) of $CoFe_2O_4$.

Sample	a (Å)	D (nm)	d_x (g/cm^3)	$\sum$
300°C	8.3946±0.0168	22.96±0.018	5.27±0.031	0.0050±0.0001
400°C	8.3644±0.0017	23.07±0.018	5.33±0.031	0.0049±0.0001
500°C	8.3471±0.0069	24.83±0.018	5.360.026	0.0046±0.0003

As seen in Table 1, a decrease with increasing annealing temperature. This finding is consistent with the previous study.[26] Moreover, $\sum$ decrease with increasing annealing temperature namely 0.0050, 0.0049 and 0.0046, respectively. However, D increase with an increase in annealing temperature (Figure 2). This might be due that increasing annealing temperature can reduce internal stress and promote crystal growth which is consistent with the previous study.[36–38] It is also shown that the crystalline density of the sample increase with annealing temperature i.e., 5.27 g/cm^3, 5.33 g/cm^3 and 5.36 g/cm^3 which is typically owing to the $CoFe_2O_4$ nanoparticles.

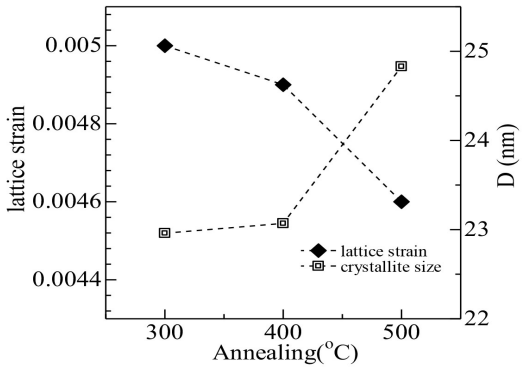

Figure 2: Annealing temperature dependence of the crystallite size and lattice strain.

Figure 3 shows FTIR spectra of $CoFe_2O_4$ at annealing temperatures of 300°C, 400°C and 500°C. It was found the presence of strong absorption bands in the range of wavenumber k = 414.71 cm^{-1} – 444.61 cm^{-1} and 568.99 cm^{-1} – 573.85 cm^{-1} attributed to the vibration of metal oxide bonds at a tetrahedral site (v_1) and octahedral site (v_2), respectively. The v_1 and v_2 indicate the absorption of the Fe-O and Co-O, respectively. This is a typical characteristic of spinel ferrite material.[39,40] Then, it was discovered that, in addition to the main IR absorption band owned by $CoFe_2O_4$ material, which is shown in Table 2, other IR absorption bands appeared in the samples from this study.

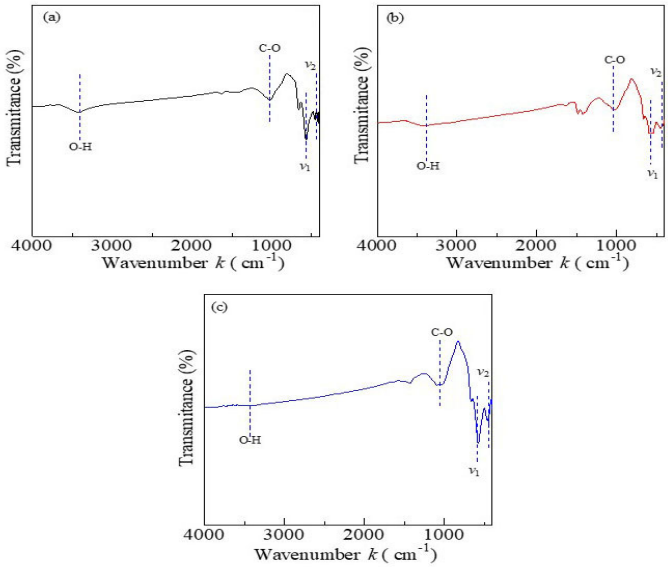

Figure 3: The typical FTIR spectra of $CoFe_2O_4$ at various annealing temperatures of 300°C, 400°C and 500°C.

Table 2: Bond analysis FTIR spectra of $CoFe_2O_4$ based on iron sand at different annealing temperatures.

Bond	Wavenumber k (cm^{-1})			Mode
	300°C	400°C	500°C	
Co–O	414.71	442.68	434.97	Stretching
Fe–O	568.99	569.03	569.03	Stretching
C–O	1,020.39	1,014.60	1,040.64	Stretching
O–H	3,412.20	3,417.40	3,427.65	Stretching

Figure 4 shows the surface morphology of $CoFe_2O_4$ nanoparticles using natural iron sand as the source of Fe cations. It was observed that the nanoparticles formed a hollow structure. The large hollow is formed at a lower annealing temperature and decreases with increasing annealing temperature. This demonstrates that an increase in annealing temperature is used when individual nanoparticles close together and then combine to form larger and more compact granules, resulting in a smaller hollow. The particle size of the $CoFe_2O_4$ nanoparticles samples made from the iron sand of the Solo River was observed to be ~100 nm larger than in previous studies.[37] It seems that the energy required for the granules to coalesce is less than that of $CoFe_2O_4$ nanoparticles synthesised with all analytical pure chemical materials as before.

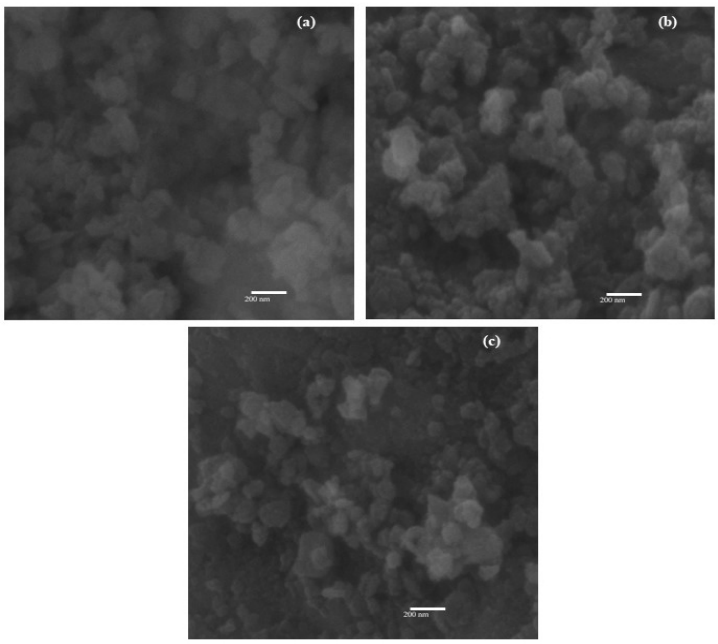

Figure 4: SEM images of coprecipitated $CoFe_2O_4$ nanoparticles with annealing temperatures of 300°C, 400°C and 500°C.

Figure 5 shows the M-H hysteresis curve of coprecipitated $CoFe_2O_4$ nanoparticles magnetic with different annealing temperatures. The magnetic-parameter properties, on the other hand, can be calculated and summarised in Table 3. Ms was obtained for nanoparticle samples at 30.8 emu/g and 30.55 emu/g after annealing at 300°C and 400°C. The Ms then decreases to 23.25 emu/g at 500°C of annealings. Moreover, the total magnetic moment, calculated using Equation (5), also showed a similar trend. The magnetic moment's n_B were 1.3 μ_B, 1.28 μ_B, and 0.98 μ_B for annealing temperatures of 300°C, 400°C and 500°C, respectively. The decrease in Ms as annealing temperature increased was similar to the previous study, although some report an increase in Ms value with increasing annealing temperature.[41–43] The difference in the results obtained was allegedly due to the characteristics of each material. Cation redistribution between octahedral sites (B-sites) and tetrahedral sites can explain a decrease in Ms (A-sites). The total magnetic moment of $CoFe_2O_4$ nanoparticles can be expressed as . Furthermore in this study, lower should result in the migration of Fe^{3+} cation from octahedral sites (B-sites) to tetrahedral sites (A-sites) and consequently decrease Ms.

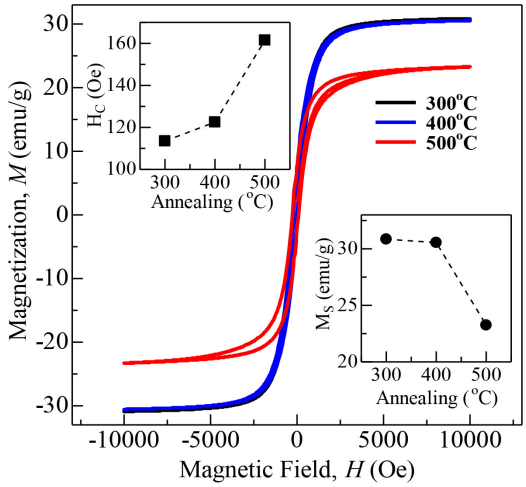

Figure 5: Hysteresis loop of $CoFe_2O_4$ nanoparticles for different annealing temperatures of 300°C, 400°C and 500°C.

Other, the coercive fields (H_C) are obtained at 113.5 Oe, 122.5 Oe and 161.5 Oe for annealing temperatures of 300°C, 400°C and 500°C, respectively. These results can be correlated with the increase in magnetic anisotropy (K_1) constants of 1.92 10^4 erg/cm^3, 2.08 10^4 erg/cm^3 and 2.09 10^4 erg/cm^3 for each annealing temperature of 300°C, 400°C and 500°C. These findings confirm that the increase in the K_1 contributes to the increase in the coercive field in this sample of $CoFe_2O_4$

nanoparticles. Another factor contributing to the increase in the H_C magnitude for this nanoparticles sample is domain wall pinning at the interface caused by a change in crystallite size.[41,44]

Table 3: Magnetic properties of coprecipitated $CoFe_2O_4$ nanoparticles for a different annealing temperature.

Sample	Ms (emu/g)	n_B (μ_B)	H_c (Oe)	K_1 (10^4 erg/cm^3)
300°C	30.85	1.30	113.5	1.92
400°C	30.55	1.28	122.5	2.08
500°C	23.25	0.98	161.5	2.09

Figure 6 shows the characteristics of $CoFe_2O_4$ nanoparticles which were annealed at 300°C as a photocatalyst to reduce MB under UV light irradiation for 10 min. The absorption peak decreased with the addition of $CoFe_2O_4$ concentration as a catalyst in the MB solution. The percentage reduction obtained for the mass of $CoFe_2O_4$ as a 5 mg photocatalyst was 28.36%. Then, for photocatalyst masses of 10 mg, 15 mg and 20 mg, the percentages gradually increased to 42.60%, 49.51% and 58.01%, respectively. This demonstrated that the $CoFe_2O_4$ catalyst used in the current study performs well as a photocatalyst material for the degradation of 20 ppm MB. Other temperature-annealed $CoFe_2O_4$ samples also showed similar photocatalytic performance (data not shown). Then the degradation efficiency of the $CoFe_2O_4$ catalyst for MB decomposition can be determined from the absorbance value by Equation (6) as depicted in Figure 7.

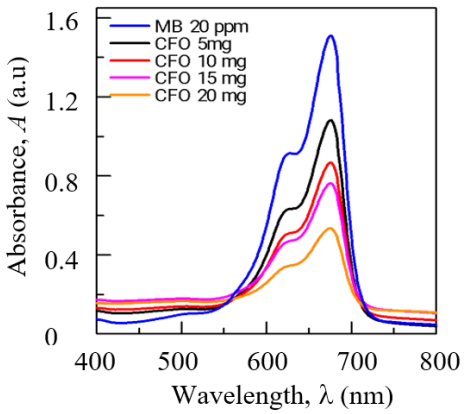

Figure 6: The photocatalytic performance of 5 mg, 10 mg, 15 mg and 20 mg $CoFe_2O_4$ nanoparticles annealed at 300°C in 20 ppm of MB under 10 min UV irradiation.

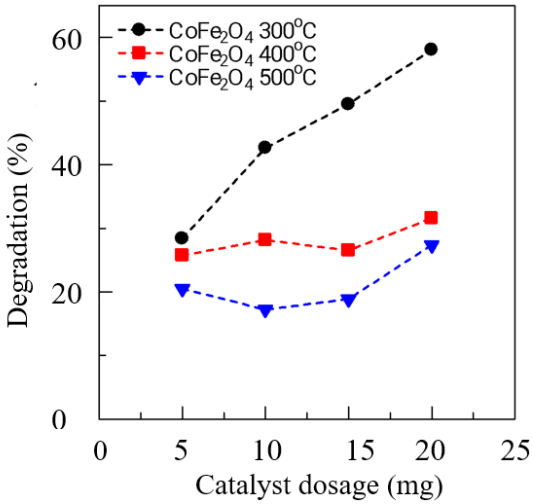

Figure 7: $CoFe_2O_4$ catalyst dosage effect with percentage degradation of MB 20 ppm.

It can be seen that the catalyst mass of 20 mg is enough to degrade the 20 ppm of MB by 58.01% for 10 min. The decrease in degradation efficiency with increased annealing temperature regarding structure properties of $CoFe_2O_4$ correlates with crystallite size. As discussed in the XRD results, the crystallite size increases with increasing annealing temperature, resulting in a decrease in surface area and as a result, a reduction in photocatalytic effectiveness. Furthermore, the SEM results show that the difference in surface morphology in the form of a hollow or granular compact determines photocatalyst efficiency. Similar to the previous study, the degradation efficiency increases as the dosage of $CoFe_2O_4$ catalyst increases.[45,46] Because many nanoparticles provide an active surface for the photocatalytic reaction to form hydroxyl radical groups (OH^*), the increase in degradation efficiency with increasing catalyst dosage may be due to the greater quantity of catalyst dosage.[47]

Furthermore, the calculation of the reaction rate can provide the desired information about the reaction. In this study, the kinetic rate constant was calculated using the first-order kinetics reaction model equation as defined in Equation (7). As a result, the kinetic rate constant of $CoFe_2O_4$ nanoparticles at a different annealing temperatures of 300°C, 400°C and 500°C for 20 ppm of MB, is depicted in Figure 8.

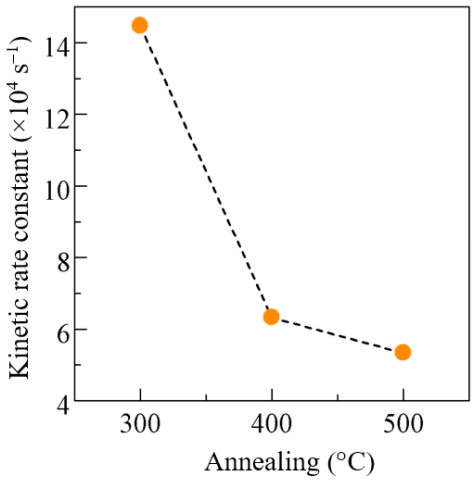

Figure 8: The kinetic rate constant of the $CoFe_2O_4$ photocatalyst.

The results showed that the kinetic rate constant decreased with annealing temperatures. This result was related to the increase of the crystallite size which caused the active surface area for photocatalytic reaction to decrease. These results agree with previous studies.[38,45]

4. CONCLUSION

The coprecipitated $CoFe_2O_4$ nanopowder was successfully synthesised and discussed the physical properties including the photocatalytic performance. Natural iron sand from the Bengawan Solo River is used as a Fe cation source for whole experiments. The structural characteristics of the FTIR results show the presence of strong metal oxide bond groups at the tetrahedral and octahedral sites, owing to the $CoFe_2O_4$ properties. The XRD pattern then confirmed the formation of a single-phase $CoFe_2O_4$ with an FCC crystal structure that closely matches reference data ICDD221086. The crystalline parameters such as lattice parameter and crystallite size change as the annealing temperature rises. The magnetic properties show that as the annealing temperature rises, the Ms decreases. Whereas the *H*c increase with the increase of annealing temperature. Thus, the annealing temperature affects the performance of the $CoFe_2O_4$ photocatalyst. It was found that the annealing temperature sample at 300°C had the best photocatalytic performance.

5. AUTHORS CONTRIBUTION

Budi Purnama: Conceptualisation, Methodology. Arga Dwi Suwandi: Data curation. Rudi Hartono: Data Curation. Sahirul Alim Tri Bawono: Data Curation. Utari Utari: Supervision. Herman Aldila: Data analysis. Adi Rahwanto: Methodology. Kusumandari Kusumandari: Data analysis

6. ACKNOWLEDGEMENTS

This study was financially supported by Penelitian Kolaborasi Perguruan Tinggi Dalam Negeri (PKPTDN) Universitas Sebelas Maret, contract number: 2400/ UN27.22/PN.01.03/2021.

7. REFERENCES

1. Shirsath, S. E. et al. (2016). Switching of magnetic easy-axis using crystal orientation for large perpendicular coercivity in $CoFe_2O_4$ thin film. *Sci. Rep.*, 6(1), 30074. https://doi.org/10.1038/srep30074
2. Shirsath, S. E. et al. (2019). Au quantum dots engineered room temperature crystallization and magnetic anisotropy in $CoFe_2O_4$ thin films. *Nanoscale Horiz.*, 4(2), 434–444. https://doi.org/10.1039/c8nh00278a
3. Shirsath, S. E. et al. (2020). Single-crystal-like textured growth of $CoFe_2O_4$ thin film on an amorphous substrate: A self-bilayer approach. *ACS App. Electron. Mater.*, 2(11), 3650–3657. https://doi.org/10.1021/acsaelm.0c00716
4. Balakrishnan, P. B. et al. (2020). Exploiting unique alignment of cobalt ferrite nanoparticles, mild hyperthermia, and controlled intrinsic cobalt toxicity for cancer therapy. *Adv. Mater.*, 32(45), 2003712. https://doi.org/10.1002/adma.202003712
5. Maksoud, M. I. A. A. et al. (2019). Antibacterial, antibiofilm, and photocatalytic activities of metals-substituted spinel cobalt ferrite nanoparticles. *Microb. Pathog.*, 127, 144–158. https://doi.org/10.1016/j.micpath.2018.11.045
6. Swathi, S. et al. (2021). Annealing temperature effect on cobalt ferrite nanoparticles for photocatalytic degradation. *Chemosphere*, 281, 130903. https://doi.org/10.1016/j.chemosphere.2021.130903
7. Kotnala, R. K., & Shah, J. (2015). Ferrite Materials. *Handbook Magnet. Mater.*, 291–379. https://doi.org/10.1016/b978-0-444-63528-0.00004-8
8. Ziaul Ahsan, Md., & Aminul Islam, Md. (2019). A theoretical approach: Effects of Mn substitution in cobalt ferrite. *Am. J. App. Sci. Res.*, 5(3), 56. https://doi.org/10.11648/j.ajasr.20190503.12
9. Saputro, D. E. et al. (2021). Tuning structural, magnetic and photocatalytic properties of bi-substituted cobalt ferrite nanoparticles. *J. Magnet.*, 26(1), 19–24. https://doi.org/10.4283/jmag.2021.26.1.019

10. Mameli, V. et al. (2016). Studying the effect of Zn-substitution on the magnetic and hyperthermic properties of cobalt ferrite nanoparticles. *Nanoscale*, 8(19), 10124–10137. https://doi.org/10.1039/c6nr01303a
11. Hashim, Mohd. et al. (2020). Structural, optical, elastic and magnetic properties of Ce and Dy doped cobalt ferrites. *J. Alloys Compd.*, 834, 155089. https://doi.org/10.1016/j.jallcom.2020.155089
12. Yadav, S. P. et al. (2015). Distribution of cations in $Co_{1-x}Mn_xFe_2O_4$ using XRD, magnetization and Mössbauer spectroscopy. *J. Alloys Compd.*, 646, 550–556. https://doi.org/10.1016/j.jallcom.2015.05.270
13. Pauthenet, R., & Bochirol, L. (1951). Aimantation spontanée des ferrites. *J. Phys. Radium*, 12(3), 249–251. https://doi.org/10.1051/jphysrad:01951001203024900.
14. Muhammad, A. et al. (2012). Large enhancement of magnetostriction due to compaction hydrostatic pressure and magnetic annealing in $CoFe_2O_4$. *J. Appl. Phys.*, 111(1), 013918. https://doi.org/10.1063/1.3675489
15. Wang, G. et al. (2018). Controlled synthesis of L-cysteine coated cobalt ferrite nanoparticles for drug delivery. *Ceram. Int.*, 44(12), 13588–13594. https://doi.org/10.1016/j.ceramint.2018.04.193
16. Tatarchuk, T. et al. (2021). Green synthesis of cobalt ferrite using grape extract: The impact of cation distribution and inversion degree on the catalytic activity in the decomposition of hydrogen peroxide. *Emergent Mater.*, 5(1), 89–103. https://doi.org/10.1007/s42247-021-00323-1
17. Kushwaha, P., & Chauhan, P. (2021). Facile green synthesis of $CoFe_2O_4$ nanoparticles using hibiscus extract and their application in humidity sensing properties. *Inorg. Nano-Met. Chem.*, 1–8. https://doi.org/10.1080/24701556.2021.1992432
18. Suwandi, A. D. et al. (2021). Comparison of crystalline structure and magnetic properties in $PbAl_xFe_{12-x}O_{19}$ synthesized by coprecipitation and sonochemistry. *J. of Phys.: Conf. Ser.*, 1825(1), 012043. https://doi.org/10.1088/1742-6596/1825/1/012043
19. Setiadi, E. A. et al. (2020). The effect of ammonia solution concentration on the synthesis process of $MgFe_2O_4$ based on natural iron sand as adsorbent of Pb ions. *AIP Conf. Proc.*, 2256, 030011. https://doi.org/10.1063/5.0015497
20. Yuliantika, D. et al. (2019). Exploring structural properties of cobalt ferrite nanoparticles from natural sand. *IOP Conf. Ser. Mater. Sci. Eng.*, 515, 012047. https://doi.org/10.1088/1757-899x/515/1/012047
21. To Loan, N. T. et al. (2019). $CoFe_2O_4$ Nanomaterials: Effect of annealing temperature on characterization, magnetic, photocatalytic, and photo-fenton properties. *Processes*, 7(12), 885. https://doi.org/10.3390/pr7120885.
22. Sun, M. et al. (2019). Synthesis and photocatalytic activity of nano-cobalt ferrite catalyst for the photo-degradation various dyes under simulated sunlight irradiation. *Mater. Sci. in Semicond. Proc.*, 91, 367–376. https://doi.org/10.1016/j.mssp.2018.12.005
23. Shirsath, S. E. et al. (2018). Ferrites obtained by sol-gel method. *Handbook Sol-Gel Sci. Technol.*, 695–735. https://doi.org/10.1007/978-3-319-32101-1_125

24. Priyadharsini, R. et al. (2023). Influence of cobalt on magnetic, dielectric and electrochemical properties of copper ferrite nanoparticles via hydrothermal method. *Solid State Sci.*, 137, 107123. https://doi.org/10.1016/j.solidstatesciences.2023.107123
25. Hadouch, Y. et al. (2022). Enhanced relative cooling power and large inverse magnetocaloric effect of cobalt ferrite nanoparticles synthesized by auto-combustion method. *J. Magnet. Magnet. Mater.*, 563, 169925. https://doi.org/10.1016/j.jmmm.2022.169925
26. Arilasita, R. et al. (2019). The effect of low-temperature annealing on the structural and the magnetic characteristics of co-precipitated strontium cobalt ferrite. *J. Korean Phys. Soc.*, 74(5), 498–501. https://doi.org/10.3938/jkps.74.498
27. Kessler, V. G. (2016). The synthesis and solution stability of alkoxide precursors. *Handbook of Sol-Gel Sci. Technol.*, 1–50. https://doi.org/10.1007/978-3-319-19454-7_1-1
28. Kulkarni, S. K. (2014). Synthesis of nanomaterials—II (Chemical Methods). *Nanotechnol. Princip. Prac.*, 77–109. https://doi.org/10.1007/978-3-319-09171-6_4
29. Jain, R. et al. (2022). Precipitating agent (NaOH and NH_4OH) dependent magnetic properties of cobalt ferrite nanoparticles. *AIP Adv.*, 12(9), 095109. https://doi.org/10.1063/5.0098157
30. Mubarok, A. T. et al. (2020). Annealing temperature effects in co-precipitated $CoFe_2O_4$ nanoparticles using Bengawan Solo River fine sediment. *Key Eng. Mater.*, 855, 64–69. https://doi.org/10.4028/www.scientific.net/kem.855.64
31. Suryanarayana, C., & Norton, M. G. (1998). *X-Ray Diffraction*. Springer. https://doi.org/10.1007/978-1-4899-0148-4
32. Basak, M. et al. (2022). The use of X-ray diffraction peak profile analysis to determine the structural parameters of cobalt ferrite nanoparticles using Debye-Scherrer, Williamson-Hall, Halder-Wagner and Size-strain plot: Different precipitating agent approach. *J. Alloys Compd.*, 895, 162694. https://doi.org/10.1016/j.jallcom.2021.162694
33. Prasetya, N. P. et al. (2023). The effect of annealing temperature on the structural and magnetic properties of lanthanum doped cobalt ferrite with the Bengawan Solo River fine sediment as the source of Fe^{3+}. *Key Eng. Mater.*, 940, 11–20. https://doi.org/10.4028/p-hr571t
34. El-Ghazzawy, E. H. & Amer, M. A. (2017). Structural, elastic and magnetic studies of the as-synthesized $Co_{1-x}Sr_xFe_2O_4$ nanoparticles. *J. Alloys Compd.*, 690, 293–303. https://doi.org/10.1016/j.jallcom.2016.08.135
35. Abbas, N. et al. (2020). Aluminum-doped cobalt ferrite as an efficient photocatalyst for the abatement of methylene blue. *Water*, 12(8), 2285. https://doi.org/10.3390/w12082285
36. Senthil, V. P. et al. (2018). Study of structural and magnetic properties of cobalt ferrite ($CoFe_2O_4$) nanostructures. *Chem. Phys. Lett.*, 695, 19–23. https://doi.org/10.1016/j.cplett.2018.01.057

37. Purnama, B. et al. (2019). Effect of calcination temperature on structural and magnetic properties in cobalt ferrite nano particles. *J. King Saud Univ. Sci.*, 31(4), 956–960. https://doi.org/10.1016/j.jksus.2018.07.019
38. Yu, L. et al. (2020). Annealing temperature on the microstructure and magnetic properties of magnesium–cobalt ferrite prepared by sol-gel self-propagating method. *J. Mater. Sci. Mater. Electron.*, 31(24), 22662–22675. https://doi.org/10.1007/s10854-020-04778-6
39. Kumar, H. et al. (2014). FTIR and electrical study of dysprosium doped cobalt ferrite nanoparticles. *J. Nanosci.*, 2014, 1–10. https://doi.org/10.1155/2014/862415.
40. Jabbar, R. et al. (2020). Structural, dielectric and magnetic properties of Mn^{+2} doped cobalt ferrite nanoparticles. *J. Magn. Magn. Mater.*, 494, 165726. https://doi.org/10.1016/j.jmmm.2019.165726
41. Nlebedim, I. C. et al. (2013). Non-stoichiometric cobalt ferrite, $Co_xFe_{3-x}O_4$ (x=1.0 to 2.0): Structural, magnetic and magnetoelastic properties. *J. Magn. Magn. Mater.*, 343, 49–54. https://doi.org/10.1016/j.jmmm.2013.04.063
42. Sanchez-Marcos, J. et al. (2018). Cation distribution of cobalt ferrite electrosynthesized nanoparticles. A methodological comparison. *J. Alloys Compd.*, 739, 909–917. https://doi.org/10.1016/j.jallcom.2017.12.342
43. Shirsath, S. E. et al. (2011). Effect of sintering temperature and the particle size on the structural and magnetic properties of nanocrystalline $Li_{0.5}Fe_{2.5}O_4$. *J. Magn. Magn. Mater.*, 323(23), 3104–3108. https://doi.org/10.1016/j.jmmm.2011.06.065
44. Kumar, G. S. et al. (2018). Synthesis and characterization of nickel-substituted cobalt ferrite nanoparticles using sol–gel auto-combustion method. *J. Supercon. Nov. Magn.*, 32(6), 1715–1723. https://doi.org/10.1007/s10948-018-4867-5
45. Ali, N. et al. (2020). Photocatalytic degradation of congo red dye from aqueous environment using cobalt ferrite nanostructures: Development, characterization, and photocatalytic performance. *Water Air Soil Pollut.*, 231(2). https://doi.org/10.1007/s11270-020-4410-8
46. Dojcinovic, M. P. et al. (2021). Mixed Mg–Co spinel ferrites: Structure, morphology, magnetic and photocatalytic properties. *J. Alloys Compd.*, 855, 157429. https://doi.org/10.1016/j.jallcom.2020.157429
47. Kirankumar, V. S. & Sumathi, S. (2018). Photocatalytic and antibacterial activity of bismuth and copper co-doped cobalt ferrite nanoparticles. *J. Mater. Sci. Mater. Electron.*, 29(10), 8738–8746. https://doi.org/10.1007/s10854-018-8890-x